Simulation studies of non-neutral plasma equilibria in an electrostatic trap with a magnetic mirror

K. Gomberoff
Center for Beam Physics, Lawrence Berkeley National Laboratory and Department of Physics, University of California, Berkeley, Berkeley, California 94720 and Physics Department, Technion, Haifa 32000, Israel

J. Fajans and J. Wurtele
Center for Beam Physics, Lawrence Berkeley National Laboratory and Department of Physics, University of California, Berkeley, Berkeley, California 94720

A. Friedman, D. P. Grote, and R. H. Cohen
Fusion Energy Program, Lawrence Livermore National Laboratory, Livermore, California 94550

J.-L. Vay
Lawrence Berkeley National Laboratory, Berkeley, California 94720

(Received 18 December 2006; accepted 19 March 2007; published online 16 May 2007)

The equilibrium of an infinitely long, strongly magnetized, non-neutral plasma confined in a Penning-Malmberg trap with an additional mirror coil has been solved analytically [J. Fajans, Phys. Plasmas **10**, 1209 (2003)] and shown to exhibit unusual features. Particles not only reflect near the mirror in the low field region, but also may be weakly trapped in part of the high field region. The plasma satisfies a Boltzmann distribution along field lines; however, the density and the potential vary along field lines. Some other simplifying assumptions were employed in order to analytically characterize the equilibrium; for example the interface region between the low and high field regions was not considered. The earlier results are confirmed in the present study, where two-dimensional particle-in-cell (PIC) simulations are performed with the Warp code in a more realistic configuration with an arbitrary (but physical) density profile, realistic trap geometry and magnetic field. A range of temperatures and radial plasma sizes are considered. Particle tracking is used to identify populations of trapped and untrapped particles. The present study also shows that it is possible to obtain local equilibria of non-neutral plasmas using a collisionless PIC code, by a scheme that uses the inherent numerical collisionality as a proxy for physical collisions. © *2007 American Institute of Physics*. [DOI: 10.1063/1.2727470]

I. INTRODUCTION

The equilibrium of a non-neutral plasma in a Penning-Malmberg trap has been the subject of many studies.[1–3] A mirror field has been suggested to cause transport in such traps.[1] Thermal equilibrium in Malmberg-Penning traps has been studied,[4] but without a detailed analysis of mirror fields. A hollow electron column with axial mirrors has also been considered.[5] Penning-Malmberg traps have been recently used in experiments for the production of antihydrogen[6,7] and are considered, with mirror fields added to confine the antihydrogen itself, for present and future experiments as well.[8–10]

Recently the effects of a multipole magnetic field intended to trap the antihydrogen radially in such a trap have been studied experimentally,[10,11] theoretically,[12] and with simulations.[13,14] This work was conducted at UC Berkeley as part of the ALPHA (Ref. 8) collaboration. Future ALPHA experiments will use a mirror field. The results presented here are not meant to study the ALPHA geometry, but, rather are motivated by the study of how the non-neutral plasma equilibrium self-consistently changes as the mirror field is applied.

These numerical studies are motivated in part by earlier work,[15] where it was shown analytically that a non-neutral plasma exhibits unusual features when a magnetic mirror field is added to the longitudinal field of the trap. In contrast to neutral plasmas, the density and potential along field lines is not constant. There are two trapping regions, one in the low field side and one in the high field side. Assuming that the velocity distribution is a Maxwellian, the density distribution obeys the Boltzmann relation (written for positrons):

$$n(z;r_L) = n(z_L;r_L)\exp\left(\frac{-e\Delta\phi(z,r_L)}{kT}\right). \tag{1}$$

Here $n=n(z;r_L)$ is the density value in along a field line originating at a radius r_L in the low field region, and $n(z_L;r_L)$ is the corresponding low field density. The potential difference along the same field line is $\Delta\phi(r;z_L)=\phi(r;z_L)-\phi(z_L;r_L)$. A typical trap configuration is shown in Fig. 1.

In Ref. 15, an infinitely long plasma is assumed and the transition between the high field and low field region is idealized via the conservation of magnetic moment. Additional assumptions were made in Ref. 15 in order to analytically characterize the equilibrium: the field variation was assumed to be small and a flat-top density profile was considered. Numerical solutions in the same paper[15] extend those results

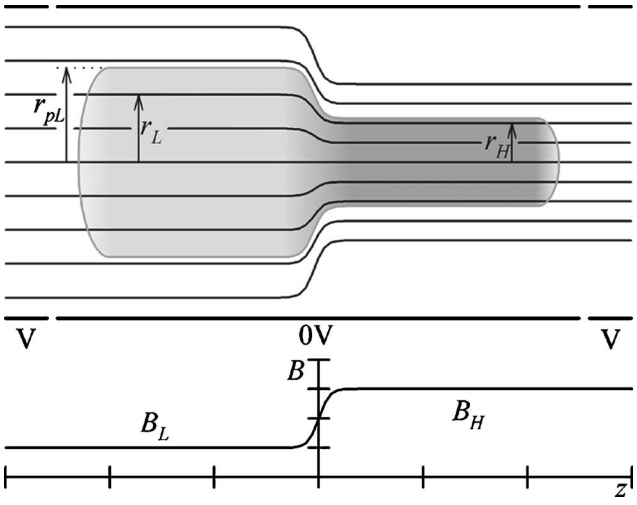

FIG. 1. Typical Penning-Malmberg trap with a mirror field. The magnetic field strength and field lines of the mirror are plotted as well as the plasma profile. r_{pl} is the initial plasma radius before the field is ramped.

to broader regimes, however still considering an infinite plasma and ignoring the transition region between high and low field. In this paper we study plasma equilibria in a realistic two-dimensional geometry with finite plasma lengths and realistic magnetic field variations. We use the WARP simulation code[16] with a two-dimensional field solver $(r-z)$. Thus, the simplifications required for the analytical study are not required. The plasma density decreases radially towards the plasma boundary. Initially the plasma is loaded, following the technique described in Refs. 13 and 14, into an equilibrium distribution which satisfies Eq. (1) along field lines in an initially uniform axial field. The mirror field is then ramped slowly until it reaches the desired value. The plasma appears to be in a new equilibrium, whose properties we investigate in detail.

We show the existence of two trapping regions and examine the deviations from constant density and potential along field lines; the Boltzmann distribution is obtained all along the field lines, including in the transition region between the high and low field, which is ignored in Ref. 15.

We previously used the same code to simulate the positron confinement in a proposed antihydrogen trap with an octupole magnetic field for the radial trapping of the antihydrogen.[13] We found that a proper equilibrium can be achieved with the Warp code, although it does not take realistic collisions into account. We employ the same techniques as in Refs. 13 and 14, in order to find the positron/electron equilibrium in the Penning-Malmberg trap with a magnetic mirror. Thus we show that by using the scheme described above, a local unknown equilibrium (with a nonuniform field) can be found from the uniform field equilibrium with a collisionless particle-in-cell (PIC) code, using the collisionality of the method to facilitate relaxation of the system.

It is not clear that a Maxwellian distribution should be obtained in PIC simulations as the result of numerical collisions. Numerical effects such as nonconservation of energy, unrealistic fluctuation levels associated with the reduced particle number, finite size macroparticles with an effective shape influenced by the grid, etc., could lead to different results. Early work by Dawson[17] showed that the plasmas modeled in a simple class of particle codes exhibit relaxation toward a Maxwellian state, as a result of three-body interactions; however, because entropy is (in general) continuously generated in PIC codes, there is formally no steady state. A detailed discussion of relaxation and related effects can be found in Chaps. 12 and 13 of Ref. 18. We intend to explore these issues more thoroughly in future work, where we hope to be able to employ the physically correct number of particles along with fine zoning. In this paper we employed a limited number of macroparticles, and so deliberately enhanced the numerical collisional effects in order to achieve more rapid damping; the Boltzmann distribution obtained as a result indicates that Maxwellization is obtained to a very large degree for the present simulation parameters.

The Warp code (Ref. 16) was designed, originally, for heavy ion beam simulations. This is a three-dimensional particle-in-cell (PIC) code that considers the self electrostatic fields of the particles, together with many external magnetic and electric field elements. One feature that makes Warp a very suitable code for the present simulations is that the time step can be larger than the gyroperiod while the various drifts and Larmor radius are calculated properly.[19] Within these strongly magnetized plasmas, the motion is primarily determined by the guiding center dynamics. Another special feature of Warp is the Python-based user programmable ("steerable") capability that enables us to, for example, gradually turn on a mirror coil or add particles during the simulation run.

The paper is organized as follows: In Sec. II the simulation setup is described. In Sec. III we present the results for different plasma configurations, namely, plasmas of different density profiles and various temperatures. In Sec. IV we discuss the particle trapping. Finally, our conclusions are given in Sec. V.

II. SIMULATION GEOMETRY AND PARAMETERS

We describe here the setup for the PIC simulations done with Warp. A representative simulation produces particles distributed in r-z as shown in Fig. 2. The trap geometry and parameters are apparent. Thus, the plasma is confined axially by two voltage rings of 100 V each. The plasma is confined radially by an axial magnetic field which, in the low field region, is 1 T. The trap wall radius is 21 mm, the plasma column width at the high field region is 7 mm. The field is approximately a factor of 2.2 higher in the high field region due to the existence of a solenoid in the right half of the plasma. The plasma length is ~300 mm and the computational field grid's spacing is 1 mm. The time step for the simulation is $1 \cdot 10^{-10}$ s. The plasma density in the low field is of the order of $1 \cdot 10^{7}$ cm^{-3}; it decreases towards its radial boundary. The initial density distribution is loaded with the previously calculated trap equilibrium. The particles have an initial Maxwellian velocity distribution. Following the technique described in Ref. 14, computational equilibrium is obtained (during hundreds of plasma periods and tens of bounce times), the mirror field is then ramped slowly (over

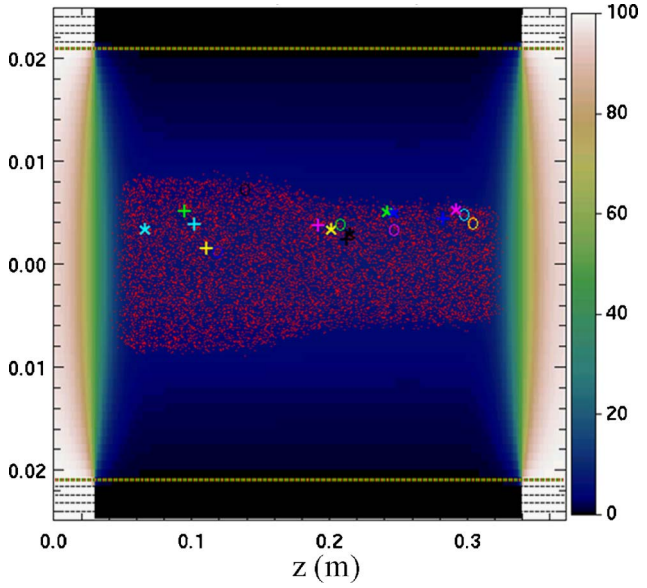

FIG. 2. (Color online) Particles (and marked particles) in the Penning-Malmberg trap with a mirror field. The potential appears as a color map. Note that only a subset of the particles is shown, in order to prevent saturation. Trapped particle orbits were observed.

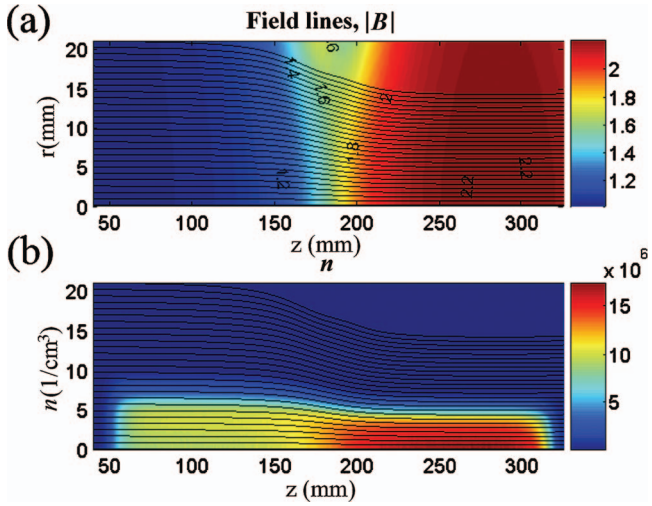

FIG. 3. (Color) (a) Color map of the magnetic field magnitude B(T) of the mirror field in the simulated non-neutral plasma trap. (b) Color map of the density ($1/\mathrm{cm}^3$) and magnetic field lines for the case of a plasma at 1 eV.

several bounce times) until it reaches the desired value, and the simulation is continued over tens to hundred of bounce times. We tracked the trajectories of selected particles; their motion along constant field lines was observed, allowing us to identify trapped particle regions and note their characteristic features.

III. PARTICLE DISTRIBUTIONS

We show here the simulation results for various density profiles and plasma temperatures. The first case is for plasma temperature of 1 eV. For these parameters the Debye length is of the order of 2.5 mm. This length is much smaller than the plasma length and significantly smaller that the plasma radius.

In Fig. 3(a) we show a color map of the magnitude of the magnetic field, together with the corresponding field lines in the r-z plane. If B_L is the magnetic field in the low field value side, and B_H is the field at the high field side, then we define β via $B_H \equiv (1+\beta)B_L$. In this simulation $\beta \approx 1.2$. The following values of the density and potential are averaged over several bounce times, in order to obtain smoother values (alternatively we could use more particles at the end of the simulation, however this usually slows down the simulation). In Fig. 3(b) we show the density color map in the r-z plane and in Fig. 4(a) we show the value of the density on the axis. In the case of a cold, infinitely long plasma with an initially flat top density distribution and for small Debye length compared to the wall radius the density should scale approximately with the field strength along the field line.[15] When comparing the density in the high field region as compared to their value in the low field, we can see from Fig. 3 that, in the interior of our plasma, for small radii (where a flat-top and infinitely long plasma is a good approximation to our initial distribution) the density scales approximately as the magnetic field. On the axis the density in the high field region is ≈ 1.9 times the low region value. In fact the density approximately scales as the magnetic field along the axis, as can be appreciated in Fig. 5. We can see that our density distribution increases along each field line over most of the plasma. In Figs. 4 and 6 we show the potential distribution. This result can appear at first sight as counterintuitive; however, the high-density region's outer radius is smaller than that of the low density region (due to the convergence of field lines), leading to a smaller potential than in the low field region, for the same field lines.[15] The potential decreases over most of the plasma region, and this is the reason that it is possible to obtain trapped particles in the high field region; they are reflected by the electrostatic potential as they move to a lower field region. Along the axis, the potential decrease is of the order of 0.4 V. However, at larger radii, there is a general trend for the potential variation along field

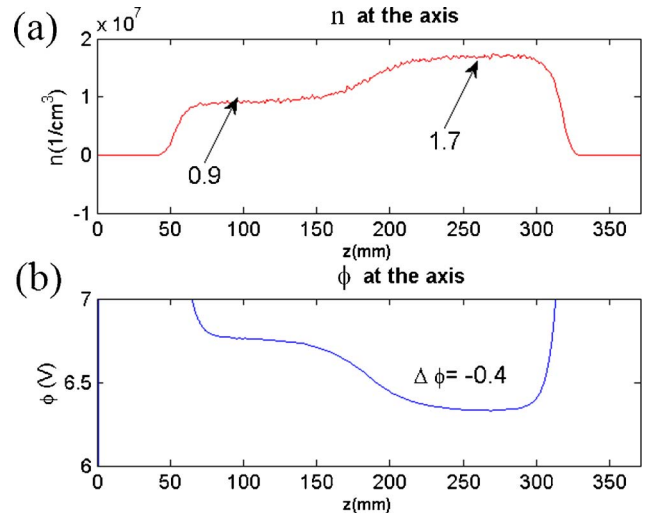

FIG. 4. (Color online) (a) The density at the axis for the case of a plasma at 1 eV. Averaged density values in the low and high field region are shown. (b) The potential at the axis for the same case.

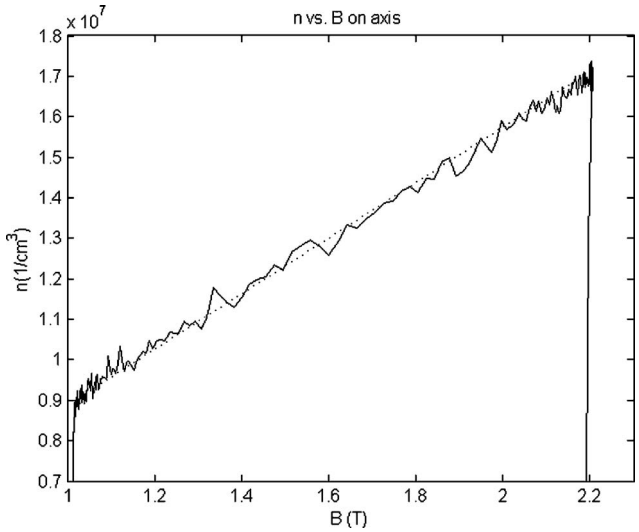

FIG. 5. The density as a function of the magnetic field at the axis for the case of a plasma at 1 eV.

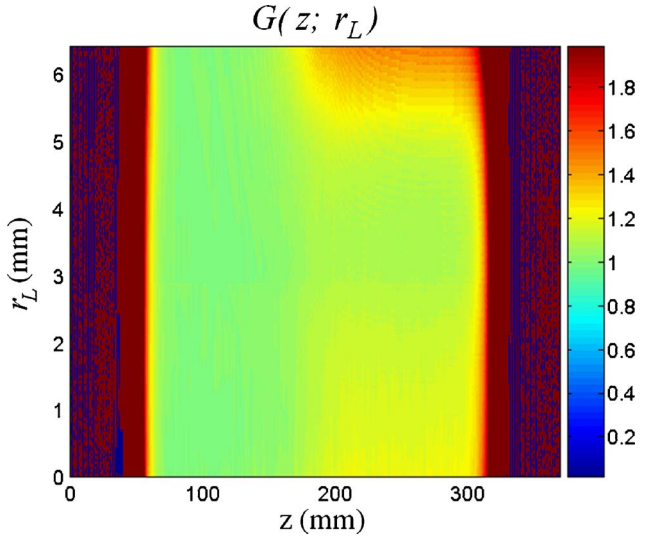

FIG. 7. (Color online) Color map of $G(z;r_L)$ for the 1 eV plasma. It should be noted that this is not a depiction of the physical r-z plane.

lines to decrease. Along a field line that originates at a radius of $\approx 7 \pm 1$ mm (marked with a dashed line in Fig. 6), the potential is constant and for larger radii it increases along field lines. We denote the field line with zero potential variation as the critical line; it defines a critical radius in both the high and in the low field regions. In the high field region particles cannot be trapped beyond the high field critical radius.

We evaluated the expression,

$$G(z;r_L) = \frac{n(r(z;r_L),z)}{n_L(r_L)\exp\left(\frac{-e\Delta\phi(r(z;r_L),z)}{kT}\right)}, \tag{2}$$

where $\Delta\phi(r,z) = \phi(r,z) - \phi(r_L)$ on each field line, which is expected to be equal to 1. In Fig. 7 we show contour maps of G in the r_L-z plane. We have interpolated the different values over a finer grid, using the "Spline" function of Matlab. G is plotted in the region where the Boltzmann distribution is satisfied. Compared to the density in Fig. 3(a), it appears that in our simulation the Boltzmann distribution is satisfied over most of the higher density region, i.e., $r_L < 6$ mm. We use the same temperature in Eq. (2) for all the plasma regions (all field lines), which in this case is of 1 eV, and is also the initial temperature that we had before ramping the mirror field. Typically, while performing the procedure for obtaining the equilibrium, the heating of most of the plasma (where the density is high), would be less than 5%. The fact that in this simulation the Boltzmann distribution is not satisfied in the region of low densities, does not mean that the Boltzmann distribution is not satisfied there; rather, we believe that the results in this region are inaccurate. The main reason for this localized inaccuracy is that there are very few macroparticles here, resulting in very large numerical noise and heating. The effective temperature in this region is thus higher and is permanently increasing for longer simulations. The use of more macroparticles is an imperfect solution. Since the equilibration process is then slower in the high density region, the simulation time becomes much longer. This leads, in turn, to more heating in the high density region. Also a differential macroparticle charge could be used according to the density, leaving the number of particles per cell uniform. This could lead to other numerical problems due to particle mixing. Since we are mainly interested in the region of higher density, we did not attempt to develop the advanced numerics nor carry out the long simulations required to analyze the boundary regions in detail.

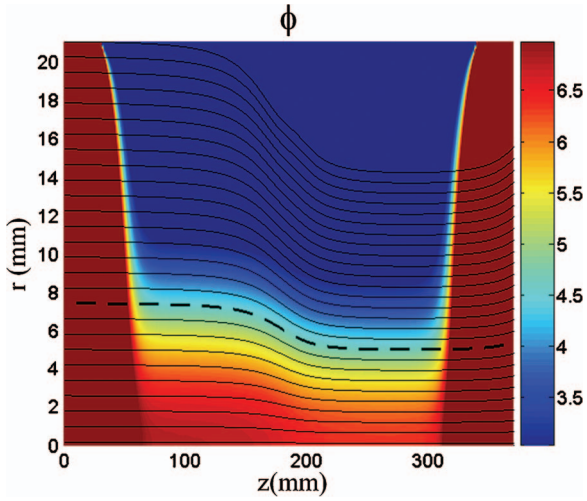

FIG. 6. (Color) Color map of the potential (V) and magnetic field lines for the case of a plasma at 1 eV.

In Ref. 15 the Boltzmann distribution was not solved for the interface between the low and high density regions. Here, in the region where the Boltzmann distribution is shown to be satisfied, we show the expected result: the Boltzmann distribution is valid along field lines. We also remark that the values of G are not trivially uniform. If, for instance, $n_L(r_L)$ is replaced by $n_L(0)$, $G(z;r_L)$ can deviate significantly from unity over most of the plasma, also if the temperature is replaced by even different values, this value deviates easily by a factor of several. Thus, for example changing the tem-

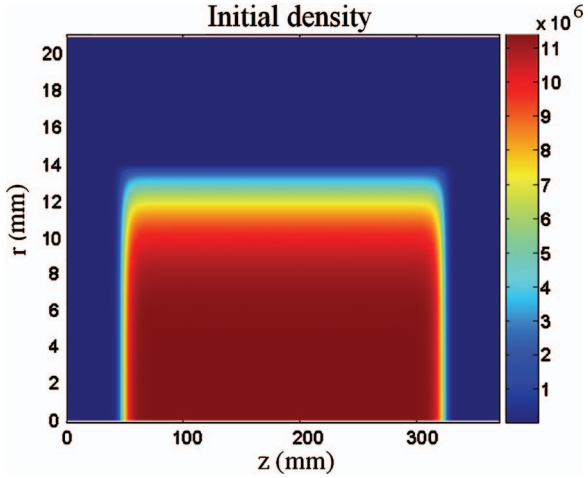

FIG. 8. (Color) Color map of the initial density distribution ($1/\mathrm{cm}^3$).

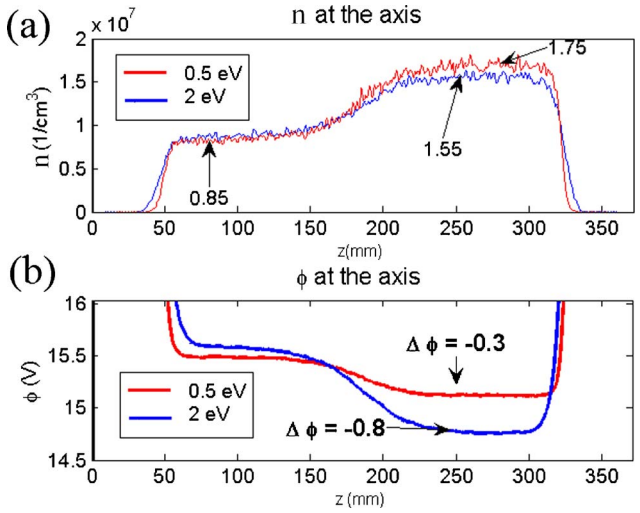

FIG. 10. (Color online) (a) The density $n(1/\mathrm{cm}^3)$ and on axis, $T=0.5$ eV and $T=2$ eV cases. Averaged density values in the low and high field region are shown. (b) The potential ϕ(V) on axis for the same cases.

perature by 50% (up or down) can lead to a change in the high to low field values of G of the same order or even more (instead of being unity), and furthermore, this value changes nonuniformly over the field lines in most of the plasma region.

We also consider two cases with a larger plasma radius (14 mm). The first case has the same plasma density as before, and a temperature of 0.5 eV. For these parameters the Debye length is even smaller, about 1.7 mm. However, we still resolve it with the grid spacing in the high density region. The second case has a higher temperature (2 eV). In Fig. 8 we show the initial density distribution for the 2 eV case. The radial falloff is clearly seen. The choice of radial profile is somewhat arbitrary since the initial Boltzmann distribution is assumed to be satisfied along field lines which are purely axial without the mirror field. Naturally, a realistic radial profile for the initial distribution has to be chosen, and our solution with mirror fields depends on this choice.

For the 0.5 eV temperature case, we expect that the density will scale as the field strength with even higher accuracy than for the higher temperatures. In Fig. 9(a), we plot the density color map and the field lines. In this case, the density on the axis is 2.05 times its value in the low field region, as can be seen from Fig. 10(a). This is close to the 2.2 ideal value for a cold plasma. In Fig. 8(b), we show the potential color map. We can see that the critical radius occurs at $r_L = 10 \pm 1$ mm. The decrease of the potential on the axis is of the order of 0.3 V [Fig. 10(b)].

In the case of a 2 eV plasma, the density increase on the axis, as expected, is somewhat smaller than in the previous cases. The density is ≈ 1.8 times larger in the high field region than in the low field region [see Fig. 10(a)]. The potential decrease along the axis is about 0.8 V [Fig. 10(b)], higher than in the colder case. In Fig. 10(a), the density color map is shown and in Fig. 11(b) the potential is plotted. We can see that the critical radius occurs at $r_L = 9 \pm 1$ mm. Clearly, as the temperature decreases the transition between the density in the low and high field region occurs on a smaller scale.

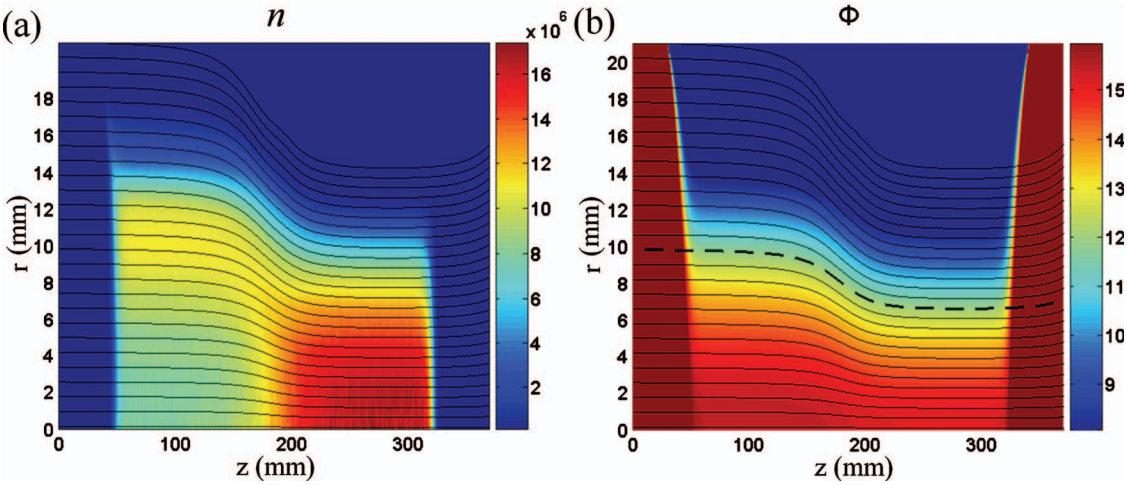

FIG. 9. (Color) (a) Color map of the density $n(1/\mathrm{cm}^3)$ and magnetic field lines for $T=0.5$ eV. (b) Color map of the potential ϕ(V) and magnetic field lines for the same plasma.

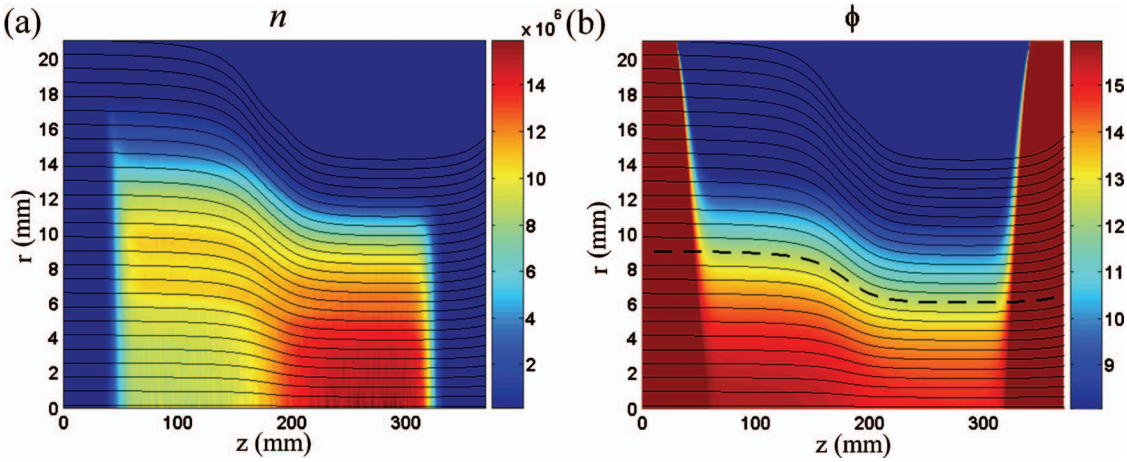

FIG. 11. (Color) (a) Color map of the density $n(1/\mathrm{cm}^3)$ and magnetic field lines for $T=2.0$ eV. (b) Color map of the potential $\phi(\mathrm{V})$ and magnetic field lines for the same plasma.

In Fig. 12 we plot color maps of the function G in the r_L-z plane for both cases. We observe that the Boltzmann equation is satisfied over a similar region in both cases. This region is roughly within the critical radius. On the plasma boundaries, there is some numerical heating, so that a rough Boltzmann distribution is satisfied, but at an increased temperature. The somewhat discontinuous lines are due to the finite grid and the existence of numerical noise.

IV. PARTICLE TRAPPING

The simulations show that some particles are trapped in the low field region, others (relatively few) are transiently trapped in the high field region, and most oscillate between the two potential barriers at the ends of the plasma. A typical untrapped particle trajectory is shown in Fig. 13. The axial position is plotted as function of time in Fig. 13(a) and the orbit in r-z is plotted in Fig. 13(b) (the orbit follows a field line).

Energy and magnetic moment conservation yields[15] a useful expression in approximation where the plasma is long, and the transition region between the high and low fields and plasma boundary are neglected:

$$V_\perp = \sqrt{\frac{1}{\beta}\left(V_\parallel^2 - \frac{2e\Delta\phi}{kT}\right)}. \tag{3}$$

Here $V_\perp$, $V_\parallel$ are the transverse and axial velocities of the particles, respectively, normalized by the thermal velocity given by $V_T=\sqrt{kT/m}$. This gives a hyperbolic shape of the separatrix between the particles trapped in the low field region and those that are untrapped. For sufficiently large perpendicular velocities particles are trapped. In case where there is zero potential variation along the field lines the separatrices reduce to the cold limit of straight lines originating at the origin. Thus, the trapping of particles is favored at larger radii, where the potential variation is smaller or even positive. At the smaller radii, the trapping is favored at lower temperatures since the potential difference is smaller. In our

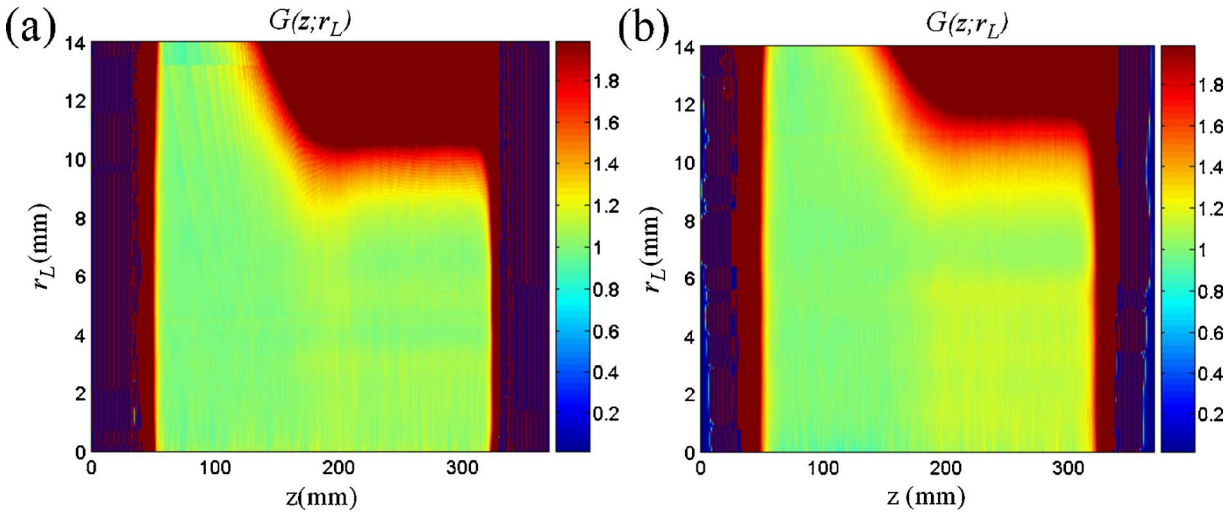

FIG. 12. (Color online). Color map of $G(z;r_L)$ [defined in Eq. (2)] for (a) $T=0.5$ eV and (b) $T=2.0$ eV.

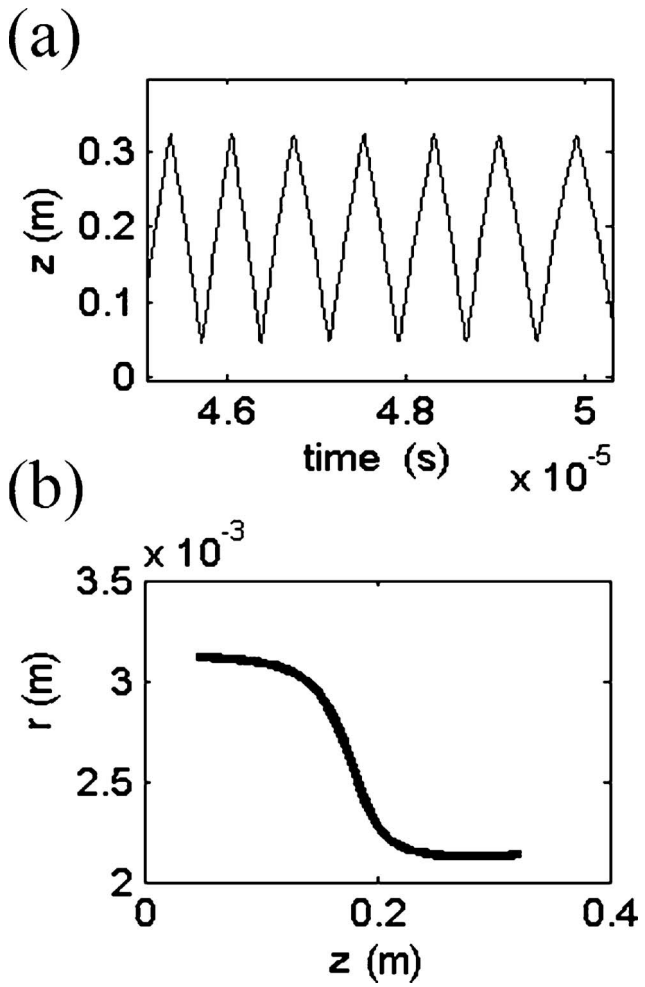

FIG. 13. Typical untrapped particle trajectory for a $T=0.5$ eV plasma: (a) axial position as a function of time; (b) particle trajectory in the r-z plane.

examples, the potential variation is, at most, of the order of 0.3–0.8 V (for the 0.5 eV–2 eV cases, respectively). For the potential term in Eq. (3), this gives a value of <0.6 in the 0.5 eV case and 0.8 in the 2 eV case. Since $\sqrt{\beta}\approx 1$, particles reflected in the low field region should have perpendicular velocity of at least the value of the parallel velocity (for radii lower than the critical radius). They can have lower values only for radii larger than the critical radius. These features are observed. There is large number of trapped particles in the low field region and more particles are trapped at larger radii (also as expected). A typical result for a trapped particle for a $T=0.5$ eV plasma is shown in Figs. 14(a) and 14(b). The particle is inside the critical radius, therefore its perpendicular velocity should be larger than its parallel velocity. Indeed, the highest parallel velocity is $5\cdot 10^5$ m/s, while the perpendicular velocity is at most $9\cdot 10^5$ m/s. The particle follows a field line trajectory.

In the high field region,

$$V_\perp = \sqrt{\frac{1+\beta}{\beta}\left(-V_\parallel^2 - \frac{2e\Delta\phi}{kT}\right)}. \tag{4}$$

This yields an elliptical shape for the separatrices, which for the analytical top hat distribution decrease in size as the radius increases. For our parameters, the value of the second term is positive only for radii less than the critical, and is relatively large only for small radii (see, for example, the potential in the 1 eV case of Fig. 6). Thus, particles can be trapped in the high field region only if the parallel velocity is sufficiently small. In Figs. 14(c) and 14(d) we show a particle reflected while traversing from the high to low field region for the 1 eV plasma. In fact, this occurs near the origin, where the potential rise in the low field region is highest. The parallel velocity of this particle is in fact small,

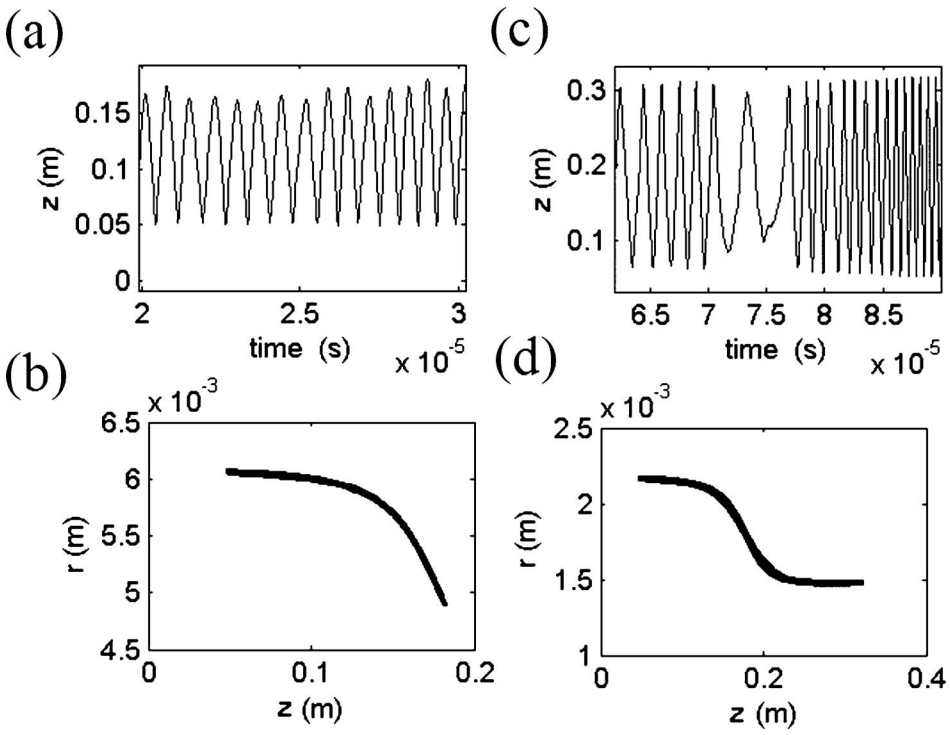

FIG. 14. Trapped particles trajectories. (a) and (b) A trapped particle orbit in the low field region in a $T=0.5$ eV plasma. (c) and (d) A particle is weakly trapped (for a few oscillations) in the high field region ($T=1$ eV). In (a) and (c) the axial position is plotted as a function of time. In (b) and (d) the radial position versus the axial position are plotted.

$3 \cdot 10^{-5}$ m/s, giving rise to a positive term in the square root in Eq. (4).

We tracked the motion of a small number (18) of particles, with randomly chosen initial conditions consistent with the initial thermal distribution. Since particles can be detrapped and trapped due to numerical collisions, the observed fraction (0.3–0.5) of trapped particles is only an estimate. This is consistent with the expected number of trapped particles in this region[15] ($\approx\sqrt{\beta/(\beta+1)}$ which is the value in the cold limit.

We observed only few particles that were trapped in the high field region (and they were trapped only for short times). This is expected to be a small fraction on the basis of the phase space analysis for the idealized case.

V. CONCLUSIONS

We have performed Warp simulations of two-dimensional plasma dynamics in a Malmberg trap with a mirror field. We use a technique to relax the simulated plasma to an equilibrium in a uniform field that was developed[14] for antihydrogen traps. We then ramp the mirror field and find numerical agreement with a basic theory that describes the equilibrium distribution in the mirror geometry. Thus, we show that the local equilibrium (with a nonuniform field) can be found from the uniform field equilibrium with a collisionless PIC code, as a consequence of the numerical noise. The Boltzmann distribution is shown to describe the plasma distribution along field lines. The density and potential need not be and are not constant along field lines. Moving beyond the earlier theory, the simulation shows that the Boltzmann distribution is satisfied in the transition region between the high and low fields. The unusual behavior of the non-neutral plasma, with some degree of trapping in both the high and low field regions, is demonstrated.

ACKNOWLEDGMENTS

This work was supported by the U.S. DOE Division of High Energy Physics, Grant No. DE-FG02-04ER41289, and by the Director, Office of Science, Office of Fusion Energy Sciences, of the U.S. Department of Energy under Contract No. DE-AC02-05CH11231, and was performed under the auspices of the U.S. Department of Energy by the University of California, Lawrence Livermore National Laboratory under Contract Nos. W-7405-Eng-48 and DEC-AC02-05, and was partially supported by the ISF (Israel).

[1] A. Kabantsev and C. Driscoll, Phys. Rev. Lett. **89**, 245001 (2002).
[2] T. M. O'Neil and C. Driscoll, Phys. Fluids **22**, 266 (1979).
[3] S. A. Prasad and T. M. O'Neil, Phys. Fluids **22**, 278 (1979).
[4] D. Dubin and T. M. O'Neil, Rev. Mod. Phys. **71**, 87 (1999).
[5] R. Davidson, A. Drobot, and C. A. Kapetanakos, Phys. Fluids **16**, 2199 (1973).
[6] M. Amoretti, C. Amsler, G. Bonomi, A. Bouchta, P. Bowe, C. Carraro, C. L. Cesar, M. Charlton, M. J. T. Collier, M. Dose, ATHENA collaboration *et al.*, Nature (London) **419**, 456 (2002).
[7] G. Gabrielse, N. S. Bowden, P. Oxley, A. Speck, C. H. Storry, J. N. Tan, M. Wessels, D. Grzonka, W. Oelert, G. Schepers, ATRAP Collaboration *et al.*, Phys. Rev. Lett. **89**, 213401 (2002).
[8] W. Bertsche, A. Boston, P. D. Bowe, C. L. Cesar, S. Chapman, M. Charlton, M. Chartier, A. Deutsch, J. Dilling, J. Fajans, ALPHA Collaboration *et al.*, "The ALPHA Experiment: A Cold Anti-Hydrogen Trap," prepared for the International Conference on Low Energy Antiproton Physics (LEAP'05), edited by D. Grzonka, R. Czyzykiewicz, W. Oelert, T. Rozek and P. Winter (American Institute of Physics, New York, 2005), Vol. 796, p. 301.
[9] W. Bertsche, A. Boston, P. D. Bowe, C. L. Cesar, S. Chapman, M. Charlton, M. Chartier, A. Deutsch, J. Dilling, J. Fajans, and ALPHA collaboration, Nucl. Instrum. Methods Phys. Res. A **566**, 746 (2006).
[10] G. Andresen, W. Bertsche, A. Boston, P. D. Bowe, C. L. Cesar, S. Chapman, M. Charlton, M. Chartier, A. Deutsch, J. Fajans, ALPHA collaboration *et al.*, Phys. Rev. Lett. **98**, 023402 (2007).
[11] J. Fajans, W. Bertsche, K. Burke, S. F. Chapman, and D. P. van der Werf, Phys. Rev. Lett. **95**, 155001 (2005).
[12] J. Fajans and A. Schmidt, Nucl. Instrum. Methods Phys. Res. A **521**, 318 (2004).
[13] K. Gomberoff, J. Fajans, A. Friedman, D. P. Grote, J.-L. Vay, and J. Wurtele, "Simulations of plasma confinement in an antihydrogen trap" (to be submitted).
[14] K. Gomberoff, J. Wurtele, A. Friedman, J.-L. Vay, and D. Grote "A method for obtaining three dimensional simulations of non-neutral plasmas using Warp," to appear in J. Comput. Phys..
[15] J. Fajans, Phys. Plasmas **10**, 1209 (2003).
[16] D. P. Grote, A. Friedman, I. Haber, and J.-L. Vay, AIP Conf. Proc. **749**, 55 (2005).
[17] J. M. Dawson, "Phys. Fluids **7**, 419 (1964).
[18] C. K. Birdsall and A. B. Langdon, *Plasma Physics via Computer Simulation* (McGraw-Hill, New York, 1985), pp. 255–303.
[19] R. H. Cohen, A. Friedman, M. Kireeff Covo, S. M. Lund, A. W. Molvik, F. M. Bieniosek, P. A. Seidl, J.-L. Vay, P. Stoltz, and S. Veitzer, Phys. Plasmas **12**, 056708 (2005).